

## Article

# The Application of Dextran Sodium Sulfate to the Efficient Separation of Ilmenite and Forsterite, as a Flotation Depressant

Guixia Fan <sup>1,2,3</sup>, Huaiyao Zhang <sup>4</sup>, Fuqiang Tian <sup>4</sup>, Hongbin Wang <sup>4</sup>, Longhua Xu <sup>4</sup> , Yijun Cao <sup>1,2,3</sup>,  
Hongxiang Xu <sup>5</sup> , Fanfan Zhang <sup>1,2,3</sup>, Jianyong He <sup>1,2,3</sup> and Guosheng Li <sup>1,2,3,\*</sup>

<sup>1</sup> Henan Critical Metals Institute, Zhengzhou University, Zhengzhou 450000, China; cumtfgx@126.com (G.F.); yijuncao@126.com (Y.C.); zhangfanfan@cumt.edu.cn (F.Z.); jianyong\_he@zzu.edu.cn (J.H.)

<sup>2</sup> Zhongyuan Critical Metals Laboratory, Zhengzhou 450000, China

<sup>3</sup> The Key Lab of Critical Metals Minerals Supernormal Enrichment and Extraction, Ministry of Education, Zhengzhou 450001, China

<sup>4</sup> School of Chemical Engineering, Zhengzhou University, Zhengzhou 450000, China; zhanghuaiyao1999@163.com (H.Z.); 17854335916@163.com (F.T.); whb7810@sohu.com (H.W.); neuxulonghua@163.com (L.X.)

<sup>5</sup> School of Chemical & Environment Engineering, China University of Mining and Technology—Beijing, Beijing 100083, China; 201535@cumb.edu.cn

\* Correspondence: lgscumt@163.com; Tel.: +86-037167781801

**Abstract:** A depressant is essential to the effective flotation-based separation of ilmenite and forsterite, based on their comparable physicochemical characteristics. In this work, dextran sodium sulfate (DSS) was initially introduced as a depressant, to aid in the separation of ilmenite and forsterite. Comparing the DSS to conventional natural starch, the results indicate that the forsterite exerts a greater depression over the ilmenite. The difference in recovery of ilmenite and forsterite was 75.44% at 10 mg/L of DSS dosage. The DSS was chemisorbed strongly onto the forsterite surface via Mg active sites, whereas its interaction with the ilmenite surface via physisorption was weak, based on the XPS and molecular-dynamics-simulation analyses. The results of the AFM and QCM-D investigations showed that the DSS adsorption layer on the forsterite surface was larger than those on the ilmenite surface. Consequently, DSS may function as a depressant, to effectively separate forsterite from ilmenite ore.

**Keywords:** flotation; dextran sodium sulfate; depressant; ilmenite; forsterite; interaction mechanisms



**Citation:** Fan, G.; Zhang, H.; Tian, F.; Wang, H.; Xu, L.; Cao, Y.; Xu, H.; Zhang, F.; He, J.; Li, G. The

Application of Dextran Sodium Sulfate to the Efficient Separation of Ilmenite and Forsterite, as a Flotation Depressant. *Processes* **2024**, *12*, 134. <https://doi.org/10.3390/pr12010134>

Received: 16 November 2023

Revised: 18 December 2023

Accepted: 26 December 2023

Published: 4 January 2024



**Copyright:** © 2024 by the authors. Licensee MDPI, Basel, Switzerland. This article is an open access article distributed under the terms and conditions of the Creative Commons Attribution (CC BY) license (<https://creativecommons.org/licenses/by/4.0/>).

## 1. Introduction

Titanium, a strategic metal, is frequently employed in aerospace, military and medical applications [1,2]. Ilmenite is an important titanium-bearing mineral, and titanite and forsterite are the primary gangue minerals in the flotation separation of ilmenite [3]. Depressing titanite/forsterite with traditional depressants is the most used flotation technique for treating ilmenite commercially. Fatty acid collectors are the next most used method [4]. Nevertheless, it is difficult to divide titanite/forsterite and ilmenite effectively, due to their comparable physicochemical characteristics [5,6].

In ilmenite ore flotation, the crucial factor is to improve the hydrophilicity of gangue minerals and modify the mineral surface property, selectively [7,8]. Previous studies reported that common inorganic depressants, like oxalic acid [9], sodium fluosilicate [10], and water glass/acidified water glass [11], exhibit some selective depressing ability for forsterite or titanite. Using chemical chelating as a depressant, oxalic acid was selectively clicked to the Ca active site of the titanite surface to produce ilmenite ore containing 26.0% TiO<sub>2</sub>. Flotation was then utilized to obtain a TiO<sub>2</sub> grade concentrate of 41.0% [9]. Acidified water glass exerts a more effective depression effect on forsterite compared to regular water glass, realizing separation between ilmenite and forsterite via flotation. Nevertheless, there

are challenges in using these depressants, including pulp acidification [11], low concentrate filtration efficiency, etc. [10,12].

Concerns over organic depressants like cellulose and starch have increased recently [13–15]. Carboxymethyl cellulose was chemisorbed on forsterite surface via Fe active sites, while it scarcely affected the collector's adsorption on the ilmenite surface [16]. Yuan et al. found that sodium citrate could be adsorbed on both the ilmenite and titanaugite surfaces, whereas sodium citrate and titanaugite interacted more strongly than sodium citrate with ilmenite [17]. Titanaugite was selectively depressed by sodium polystyrene sulfonate, resulting in a successful separation with a  $\text{TiO}_2$  grade of 42.43% and recovery of 80.87% [12]. Meng et al. illustrated that the interaction between carboxymethyl starch and the titanaugite surface inhibited the adsorption of the NaOL collector [18]. Unfortunately, most of the high-molecular polymer depressants are faced with challenges; for example, low solubility and poor dispersion in water [19].

The sulfuric acid group has the characteristics of a strong polar selective bond to metal atoms [12]. Herein, dextran sodium sulfate (DSS), with good solubility and dispersion in water, would act as a depressant to prevent forsterite and ilmenite from being separated effectively by flotation. Nevertheless, there is very little information available regarding the use of DSS in the flotation process for the separation of forsterite and ilmenite.

In this work, the depression of DSS on the forsterite and ilmenite was investigated. The micro-flotation and actual ore flotation test were used to examine the DSS's inhibitory performance. The adsorption of DSS on the surface of forsterite and its effect on the adsorption of sodium oleate (collector) were further investigated, using zeta potential measurement (Malvern Hills District Britain), X-ray photoelectron spectroscopy (XPS, Thermo 250 XI, Waltham, MA, America), Fourier-transform infrared spectroscopy (FT-IR, Nicolet Nexus 670, Waltham, MA, America), atomic force microscopy (AFM, Bruker, Karlsruhe Hadstrae, Germany), in situ quartz crystal microbalance with dissipation monitoring (QCM-D, Biolin Scientific, Gothenburg, Sweden), and molecular dynamics simulation analysis. A potential reaction mechanism was created in order to gain greater insight into the adsorption of sulfate groups at the forsterite/water interface.

## 2. Experimental Section

### 2.1. Materials

The pure ilmenite (Figure 1a) and forsterite ore (Figure 1b) were collected from Panzhihua, Sichuan Province, China. The sample fraction of 38~74  $\mu\text{m}$  was chosen for micro-flotation, whereas the  $-38 \mu\text{m}$  fraction was utilized for mechanism characterization, after being further ground to  $-5 \mu\text{m}$ .

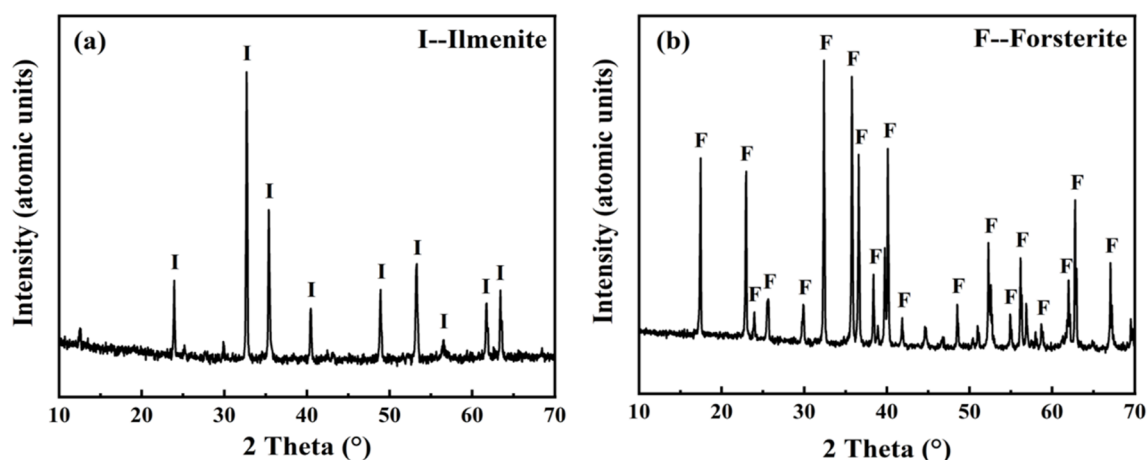


Figure 1. X-ray diffraction patterns of (a) pure-ilmenite and (b) forsterite samples.

The DSS (Shanghai Macklin Biochemical Co., Shanghai, China, M.W 500000) and traditional natural starch (Shanghai Macklin Biochemical Co., Shanghai, China) were used as depressants for flotation. The collector used was sodium oleate (Shanghai Macklin Biochemical Co., Shanghai, China). The pH was adjusted to the correct level using NaOH and H<sub>2</sub>SO<sub>4</sub> (95~98%, the concentration volume fraction is 10%). All of the experiments used analytical-grade, deionized water (18.20 MΩ cm).

## 2.2. Characterization of DSS

A total of 0.05 g DSS was hydrolyzed in hydrochloric acid solution for 10 h and prepared as a 5 mg/L solution. The degree of substitution (DS) of DSS was calculated by the following formula:

$$DS = (1.62 \times S)/(32 - 1.02 \times S) \quad (1)$$

where DS is the degree of substitution; S is the sulfur content expressed in DSS.

The sulfate content was detected using ion chromatography (IC, Dionex Aquion, Sunnyvale, CA, USA). Separation and resolution of ions was carried out on an AS11-HC separation column. Conductivity was suppressed with an AERS-4 mm suppressor. The suppressor voltage and flow rate were set at 75 mA and 1.0 mL/min, and the eluent was 30 mM sodium hydroxide solution. The functional groups of DSS were analyzed using FT-IR. Following a mixture of 1.0 mg DSS and 100.0 mg KBr, measurements were taken between 400 and 4000 cm<sup>-1</sup>. A gel permeation chromatography (GPC, Agilent, 5301 Stevens Creek Blvd USA) analysis was performed to determine the average molecular weight of DSS.

## 2.3. Flotation Tests

A total of 40 mL of deionized water and 2.0 g of pure mineral were added to the cell, and the mixture was stirred at 1700 rpm [18,19]. The pulp was gradually mixed with the pH regulator, the depressant and the NaOL collector (preparation concentration 2 g/L), added after 2 min of stirring. Every reagent required 2 min of conditioning. A further 3 min was spent on the flotation time, after that.

NaOH or H<sub>2</sub>SO<sub>4</sub> solution was used to correct the pulp's pH, and stirring was continued for another 2 min. The depressant and collector were added into the pulp in sequence, and were conditioned for 2 min, separately. A further 3 min was spent on the flotation time, after that. Following drying, the concentrate and tailings underwent separate weight measurements, to ascertain the recoveries. The selectivity index (SI), calculated by the following formula [20,21], was employed to assess how DSS affected the selective separation of ilmenite and forsterite.

$$SI = \sqrt{\frac{\varepsilon_C^I}{\varepsilon_T^I} \times \frac{\varepsilon_T^F}{\varepsilon_C^F}} \quad (2)$$

The SI denotes the selectivity index, where  $\varepsilon_C^I$  and  $\varepsilon_C^F$  denote the recoveries of ilmenite and forsterite in froth products, while  $\varepsilon_T^I$  and  $\varepsilon_T^F$  represent the recoveries of ilmenite and forsterite in tailings products.

The actual minerals used for flotation in the laboratory were taken from the iron tailings of a titanium concentrator in Panzhihua, which primarily contained ilmenite and forsterite. A 0.75 L-capacity flotation machine was utilized for the roughing step of the actual ore flotation process, 225 g of actual ore (pulp concentration of 30 wt%) was placed in a flotation cell, and the pH was adjusted and stirred for 5 min. After that, the procedures were the same as for flotation of a single mineral, and the flotation time increased to 5 min. The final result of the flotation test was determined by averaging the three repetitions.

## 2.4. Interaction Mechanisms

A total of 40 mL of deionized water was used to disperse 30.0 mg of pure materials with a particle size of ~5 μm. Prior to adding DSS depressant into the pulp, the pH was adjusted to the desired value with NaOH or H<sub>2</sub>SO<sub>4</sub> solution [22,23]. The pulp was

sonicated and dispersed for 10 min; this was followed by allowing the suspension to stand for 48 h [5]. The Zetasizer Nano ZS90 device was used to measure the zeta potential of the supernatant at various pH levels. The adsorption density and standard adsorption free energy ( $\Delta G^0_{\text{ads}}$ ) of DSS on mineral surfaces were determined based on the Stern–Grahame equation [18,24].

Using 40 mL deionized water (with or without DSS depressant) and a 2.0 g sample at pH = 5.0, the mixture was stirred for 3 min. After filtering, the samples were cleaned with the deionized water, followed by drying at 50 °C for 12 h [25]. A total of 1.0 mg of the prepared samples was combined with 100.0 mg spectroscopic-grade KBr, and was then recorded in the range of 400–4000  $\text{cm}^{-1}$ , using FT-IR and XPS at pass energy of 30 eV.

After 3 min of immersion in a DSS solution (10 mg/L), the chips were rinsed with deionized water to remove any remaining reagents on the forsterite and ilmenite surfaces. After that, the chips were blasted dry using high-purity nitrogen, so that they could be scanned using AFM in contact mode at room temperature.

The dynamic adsorption behavior of the DSS on the mineral sensor at 25 °C was investigated using the QCM-D experiment. Once the deionized water had been pumped into the flow cell until the baseline was smooth, the DSS solution (10 mg/L) was added. The entire experiment was performed at pH = 5.0, at a flow rate of 0.15 mL/min. Every 0.5 s, the frequency (F) and dissipation (D) were measured. From these graphs, the mass density and thickness of the adsorbed layer were calculated.

## 2.5. Molecular Dynamics Simulation

### 2.5.1. DSS Molecule and Mineral Crystal Structure

A visualizer module from Materials Studio was used to construct the DSS molecule and mineral crystals, which were then optimized by selecting the B3LYP function of the Dmol3 module. The charge distribution was assigned to each atom in the DSS molecule, using energy optimization calculations. The structures of the DSS and mineral crystals [26,27] are displayed in Figure 2.

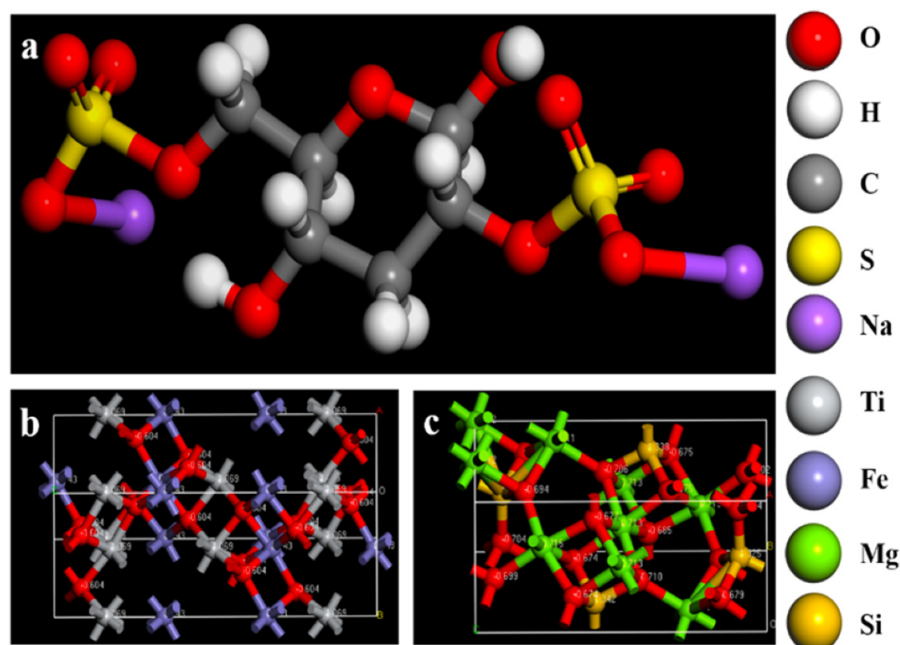


**Figure 2.** The structures of (a) DSS molecule, (b) ilmenite crystal, and (c) forsterite crystal.

### 2.5.2. Dynamics Simulation Details

Molecular dynamics simulation provides a means of quantifying intermolecular and interatomic forces [28]. The universal force field (UFF) was chosen to simulate the interaction of the ilmenite/forsterite surface with DSS [23,29]. The adsorption models were

constructed using the PCFF interface field to produce the ilmenite (101) and forsterite (010) surfaces. A total of 500 water molecules were supplied to the mineral surfaces, using the AC module to bring it closer to flotation conditions. The four DSS molecules were placed oriented to the mineral surface. To remove periodic boundary conditions, a 10 Å vacuum layer was taken into consideration in each simulation box. The details of setting parameters were based on previous reports [30].

### 3. Results and Discussion

#### 3.1. Characterization of DSS

As depicted in Figure 3a, the sulfate content of the DSS solution was found to be 2.74 mg/L, using ion chromatography. The DS of DSS was found to be 2.21, using Formula (1), indicating that the polarity and selectivity of the DSS was enhanced [4].

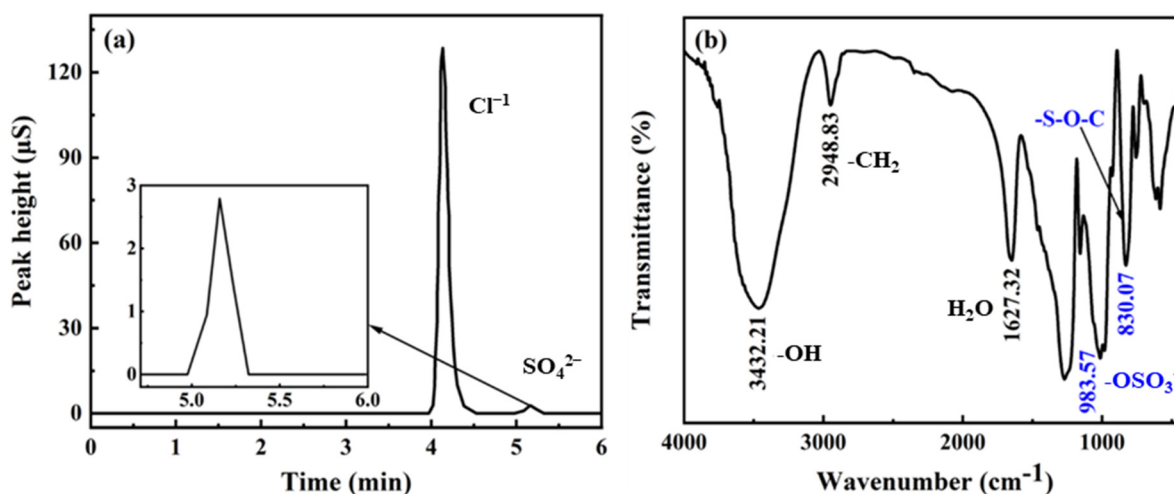


**Figure 3.** (a) The sulfate content in DSS, (b) FT-IR spectrum of DSS.

As depicted in Figure 3b, the stretching vibration of  $\text{-OH}$  and  $\text{-CH}_2$  was responsible for the two peaks, at  $3432.21\text{ cm}^{-1}$  and  $2948.83\text{ cm}^{-1}$  [31,32]. The peak at  $1627.32\text{ cm}^{-1}$  originated from tightly bound water [33]. The peaks located at  $983.57\text{ cm}^{-1}$  and  $830.07\text{ cm}^{-1}$ , respectively, were associated with the  $\text{-OSO}_3^-$  and  $\text{-S-O-C}$  groups [34]. According to GPC analysis, the DSS's average molecular weight was approximately 8899 Da, which helped the dispersion in the pump to enhance its depression performance.

#### 3.2. Flotation Experiments

##### 3.2.1. Micro-Flotation of Single Minerals

Figures 4 and 5 show the recoveries of forsterite and ilmenite at different pH values and depressant doses, respectively. As depicted in Figure 4, ilmenite and forsterite exhibited excellent flotation performance at  $\text{pH} = 5.0$  with NaOL alone. In these circumstances, ilmenite and forsterite showed a marginally different rate of recovery. The recovery of forsterite at  $\text{pH} = 5.0$  was immediately reduced, from 64.29% to 8.12%, with the addition of 10 mg/L DSS before NaOL, whereas the floatability of ilmenite was rarely affected [16,35]. As displayed in Figure 4b, both ilmenite and forsterite in recovery decreased rapidly, after natural treatment.

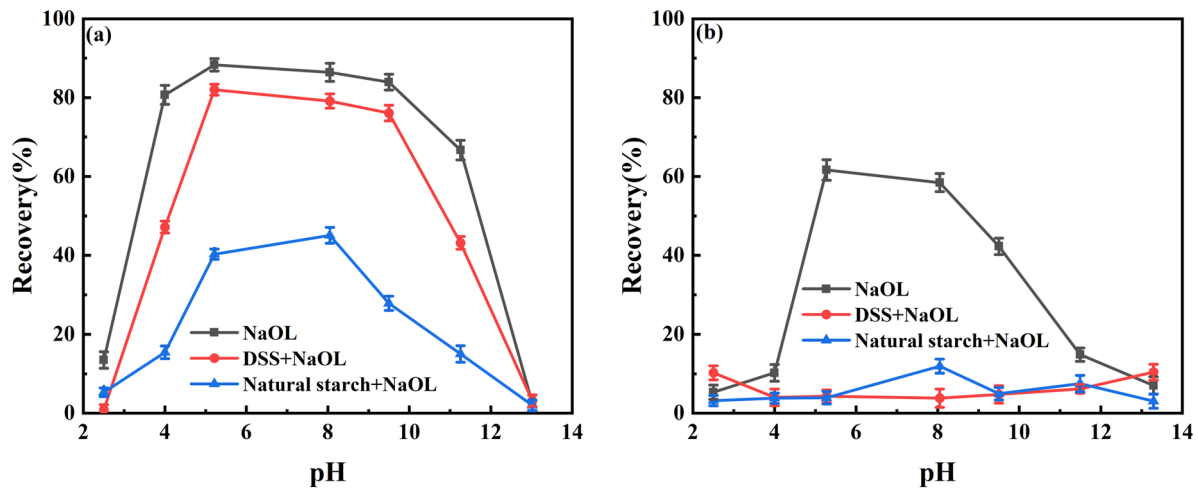


Figure 4. Effect of pH on the flotation performance of (a) ilmenite and (b) forsterite, with or without DSS ( $C_{\text{NaOL}} = 6 \times 10^{-4}$  mol/L).

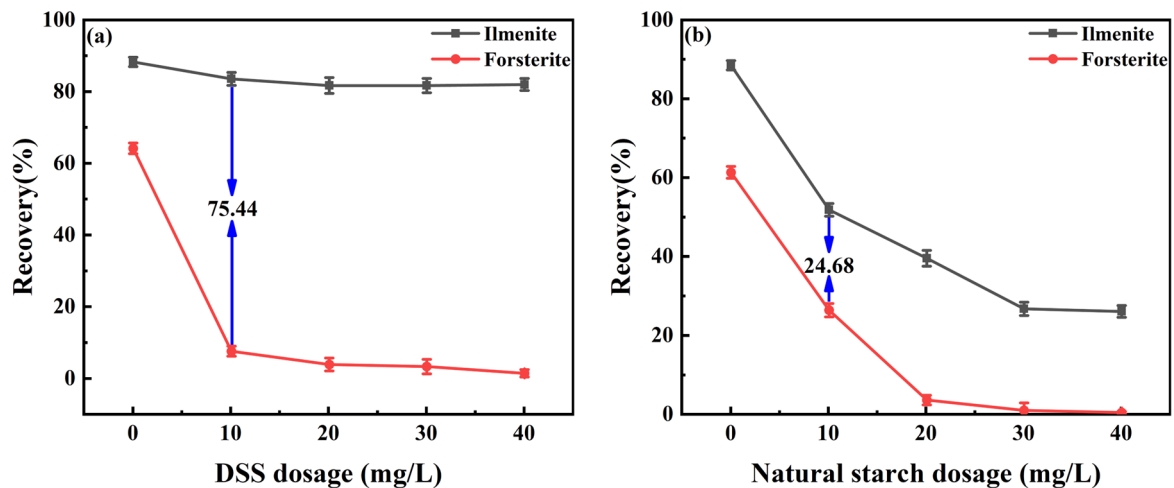
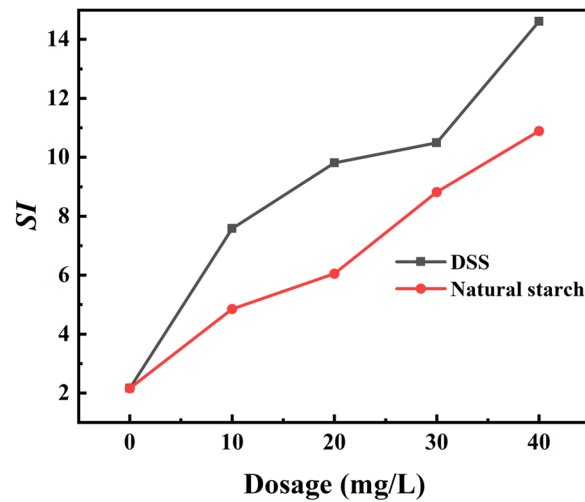


Figure 5. Effect of (a) DSS and (b) natural starch dosage on the flotation of ilmenite and forsterite at pH 5.0 ( $C_{\text{NaOL}} = 6 \times 10^{-4}$  mol/L).

As illustrated in Figure 5, the forsterite recovery met a significant decrease as the DSS dosage increased, whereas this had minimal influence on the ilmenite flotation. With the escalation of the DSS dosage to 10 mg/L, the forsterite recovery rapidly declined from 64.29% to 8.12%, while 83.56% of ilmenite was still recovered. The ilmenite and forsterite recovery declined quickly with the increasing amount of natural starch, as illustrated in Figure 5b. At a dosage of 10 mg/L of DSS, there was a 75.44% recovery differential between ilmenite and forsterite, while that of natural starch was only 24.68%.

When the DSS dosage was increased from 0 to 10 mg/L, as shown in Figure 6, the *SI* of DSS increased more quickly than that of natural starch. The *SI* of DSS with 7.58 was approximately 1.6 times that of natural starch, with 4.85 at 10 mg/L of DSS dosage. These results confirmed that the natural starch is inferior to DSS for the selective depressant flotation separation of ilmenite and forsterite.



**Figure 6.** The selectivity index of DSS and natural starch at pH = 5.0.

### 3.2.2. Laboratory Flotation of Ilmenite Ore

More research is required to determine how well DSS inhibits multi-component pulp [36]. Thus, we conducted actual ore flotation tests. As seen in Figure 7, there is a positive correlation between the  $\text{TiO}_2$  grade in the concentrate and the DSS dosage, and the recovery rate falls as the DSS dosage increases. At lower dosages, DSS has superior selective-inhibition performance. The  $\text{TiO}_2$  grade and  $\text{TiO}_2$  recovery of the concentrate are 41.21 wt% and 68.80 wt%, respectively, upon the addition of 70 g/t DSS. Therefore, it is advantageous to achieve the separation of ilmenite and forsterite when the dosage of DSS is 70 g/t.

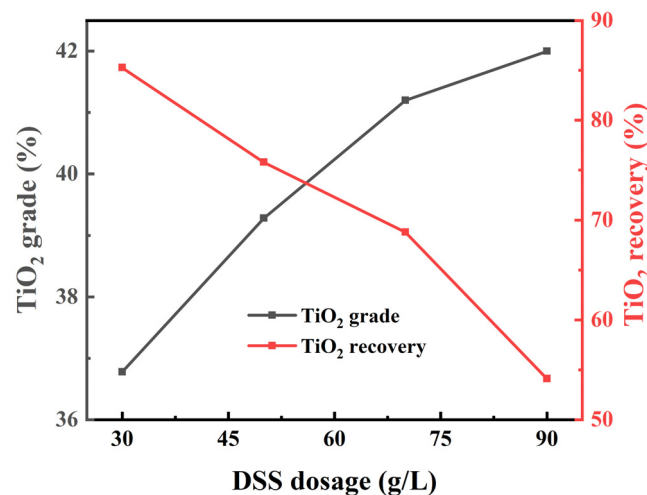


**Figure 7.** Effect of DSS dosages on the flotation concentrate ( $\text{CH}_2\text{SO}_4 = 1800$  g/t,  $C_{\text{MOH}} = 2200$  g/t).

During the ilmenite flotation process, the collector's surface is prevented from further adsorption by the highly selective inhibitor, which interacts preferentially with the metal sites on the gangue minerals. This decreases the floatability of the ilmenite, substantially. The mechanism of the inhibitor–mineral solid–liquid interface interaction is described in the following section.

## 3.3. Interaction Mechanisms of the DSS on Ilmenite/Forsterite Surface

### 3.3.1. Electrostatic Interaction Analysis

As displayed in Figure 8, both forsterite and ilmenite treated with DSS had a similar degree of negative zeta potential change. Ilmenite treated with DSS demonstrated a

negative change in its zeta potential of 11.56 mV at pH = 5, increasing from  $-4.24$  mV to  $-15.80$  mV. Similar to ilmenite, forsterite's zeta potential shifted by 9.60 mV in a negative direction. The  $\Delta G_{\text{ads}}^0$  of DSS on the forsterite surface with  $-0.93$  kJ was similar to that of ilmenite, with  $-1.12$  kJ (Table 1). These results demonstrated that DSS could interact with both ilmenite and forsterite through electrostatic interaction.

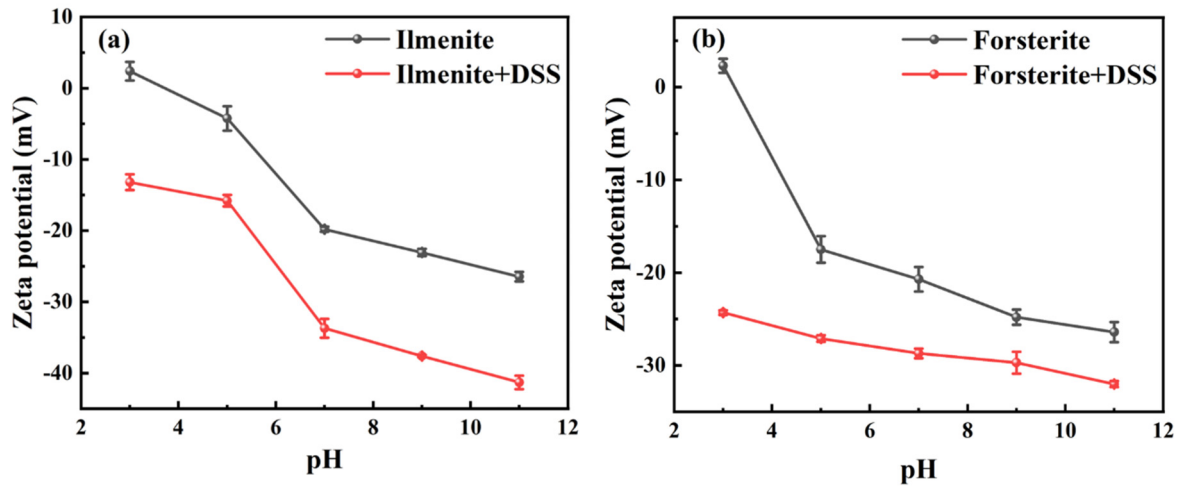


**Figure 8.** Effect of pH on the zeta potentials of (a) ilmenite and (b) forsterite, in the absence and presence of DSS.

**Table 1.** Adsorption density and standard adsorption free energy of DSS on ilmenite and forsterite surface at pH = 5.0.

Sample	$\xi_2$ (mV)	$\xi_1$ (mV)	$\Delta \xi $ (mV)	$\tau_s$ (mol/L)	$\Delta G_{\text{ads}}^0$ (kJ)
Ilmenite	$-15.80$	$-4.24$	11.56	$K \times \exp(0.01156)$	$-1.12$
Forsterite	$-27.10$	$-17.50$	9.60	$K \times \exp(0.00960)$	$-0.93$

### 3.3.2. Changes in Mineral-Surface Functional Groups before and after DSS Treatment

As shown in Figure 9, the stretching vibration of  $-\text{OH}$  on DSS appeared at  $3432.21$   $\text{cm}^{-1}$  [31]. At  $2948.83$   $\text{cm}^{-1}$ , and the  $-\text{CH}_2$  stretching vibration peak appeared [32]. Tightly bound water was identified as the cause of the band at  $1627.32$   $\text{cm}^{-1}$  [33]. The  $-\text{OSO}_3^-$  and  $\text{S}-\text{O}-\text{C}$  groups were identified as the two peaks at  $1014.40$   $\text{cm}^{-1}$  and  $830.07$   $\text{cm}^{-1}$ , respectively [34].

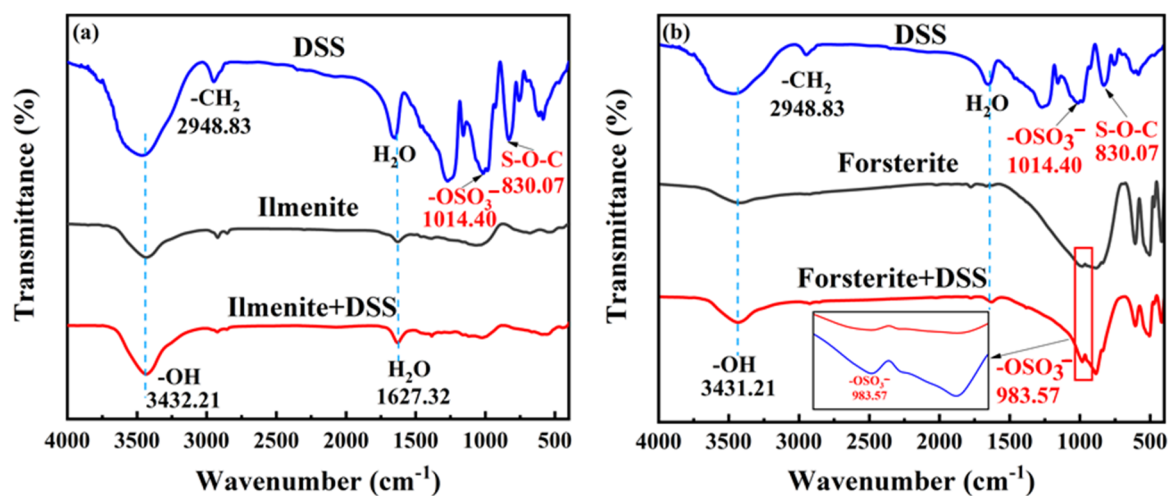


**Figure 9.** FT-IR spectra of (a) ilmenite and (b) forsterite, in the absence and presence of DSS.

Comparing the FT-IR spectra of the DSS-treated ilmenite to those of pure ilmenite, as shown in Figure 9a, no new peak was observed. These results could support the fact that the DSS was most likely to be adsorbed on the ilmenite surface via physisorption, such as intramolecular hydrogen bonds [18]. As shown in Figure 9b, a new peak at  $983.57\text{ cm}^{-1}$  was observed on forsterite surface treated with DSS, belonging to the stretching vibration of the  $-\text{OSO}_3^-$  group [34]. The significant change in the  $-\text{OSO}_3^-$  group in the DSS from  $1014\text{ cm}^{-1}$  to  $983.57\text{ cm}^{-1}$  confirmed that there was strong DSS chemisorption on the forsterite surface [37,38].

### 3.3.3. Surface Morphology Analysis

The surfaces of ilmenite and forsterite, as shown in Figure 10a,c, were smooth, with an average roughness (Ra) of 0.444 nm and 0.400 nm, which reduced the effect of the adsorption morphology study [37]. As shown in Figure 10a,b, the adsorption layer height of DSS on the ilmenite surface witnessed an increase of 8.39 nm (2D height images), and sporadically distributed bulges appeared on the 3D images. Compared with pure forsterite, the DSS bulges became clearly visible on the surface of the treated one (Figure 10c,d). Moreover, the data presented in Figure 10b,d provided enough evidence to support the variation in DSS adsorption on mineral surfaces. The 3D images showed that DSS exhibited a denser adsorption layer on the surface of forsterite than those on the ilmenite surface. Furthermore, on the forsterite surface, the DSS adsorption density and layer height were greater than on the ilmenite surface. These findings demonstrated that, compared to the ilmenite surface, the forsterite surface was more significantly absorbed by the DSS.

### 3.3.4. Changes in the Binding Energy of Minerals with/without DSS Treatment

The forsterite surface exhibited a significant increase of 3.50%, while the ilmenite surface showed a relative increase of 0.46%, after being exposed to DSS (Table 2). This confirmed that DSS had a stronger adsorption on the forsterite than ilmenite. The O1s spectra of ilmenite treated with DSS fit rather well, according to Figure 11a,b, where two factors were ascribed to the Ti-O and Fe-O bonds, respectively [39,40]. The forsterite surface's oxygen chemical environment underwent a significant change, as seen by the 0.32 eV shift in the binding energies of the Mg-O bond (Figure 11c). Moreover, compared with the high-resolution O1s spectra of pure forsterite, the newly binding energy at around 532.81 eV was observed in the treated one, which was assigned to the Mg-O-S bond [41] (Figure 11d). These results confirmed that DSS interacted with the forsterite surface through chemisorption.

**Table 2.** Relative atomic content of the elements on the ilmenite and forsterite.

Samples	Relative Atomic Content of the Elements (%)							
	C	O	Fe	Si	Ti	Mg	Ca	Al
Ilmenite	19.09	57.42	9.74	5.35	8.40	—	—	—
Ilmenite + DSS	19.55	56.36	10.63	7.17	6.29	—	—	—
Forsterite	13.52	48.04	1.83	12.74	—	14.53	6.20	3.14
Forsterite + DSS	17.02	46.18	1.88	13.56	—	12.26	5.95	3.15

As displayed in Figure 12a,b, the high-resolution Ti1s spectra of the treated and raw ilmenite have two components. Notably, there are subtle shifts in the binding energies of these bonds. Moreover, the Ti relative content decreased by 2.11% (Table 2). These results indicated that DSS was most likely to interact with the ilmenite surface through weak physisorption, such as intramolecular hydrogen bonds [14,33]. The Mg1s high-resolution spectra of forsterite may be matched rather well with two bonds;  $\text{Mg}^{2+}$  was identified as the source of the peak at 1303.42 eV [42] and Mg-Si as the source of the peak at 1304.90 eV [43] (Figure 12c). Compared with the high-resolution Mg 1s spectra of pure forsterite, as shown in Figure 12d, the newly binding energy at 1303.93 eV was observed in the treated one,

which was assigned to the Mg-O bond [44]. Furthermore, the Mg relative content was decreased by 2.27% (Table 2). These results confirmed that DSS interacted with Ti active sites on the ilmenite surface via physisorption, and chemisorbed on the forsterite surface via Mg active sites.

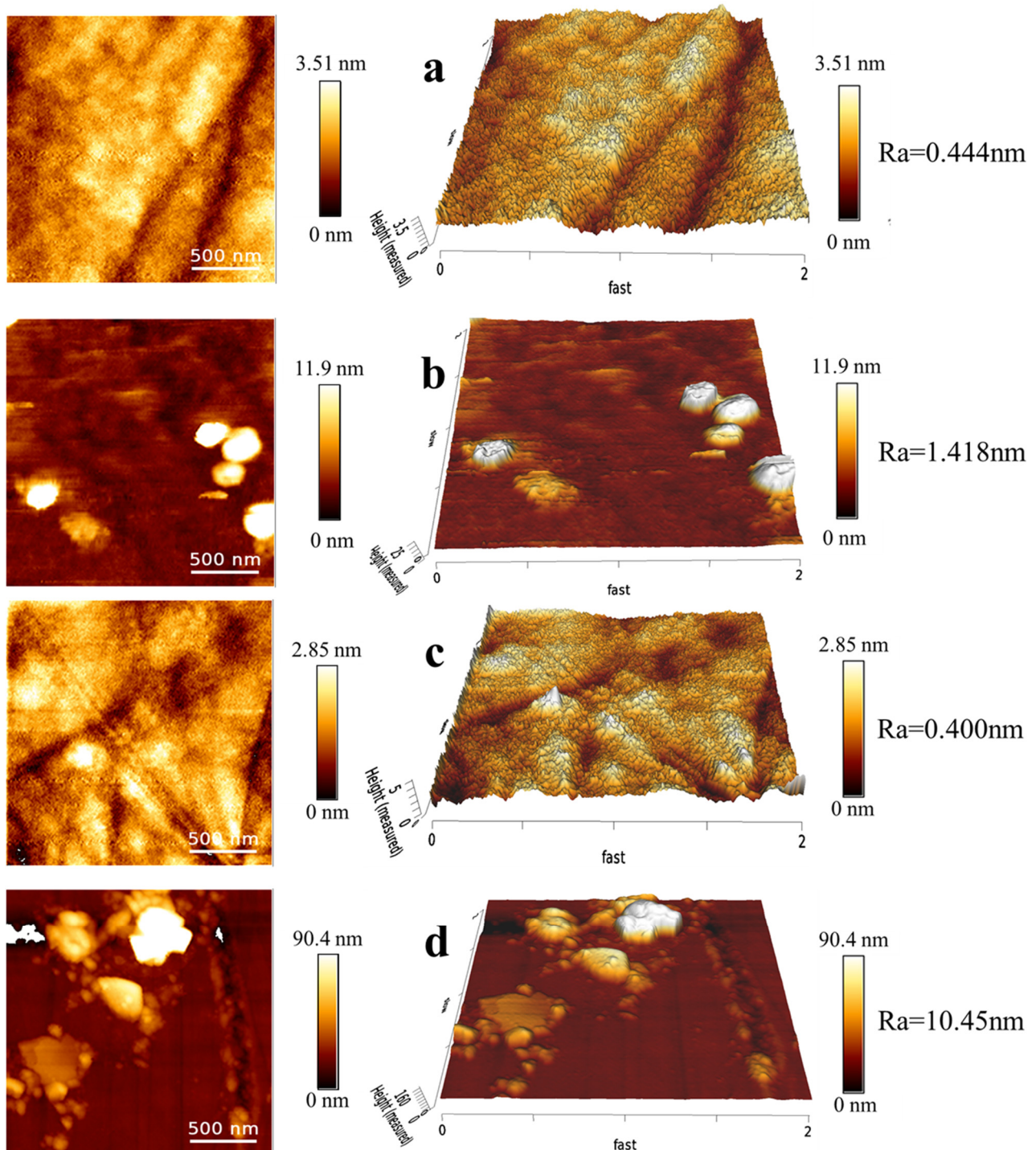


**Figure 10.** 2D and 3D images of mineral surfaces: (a) ilmenite, (b) ilmenite + DSS, (c) forsterite, and (d) forsterite + DSS.

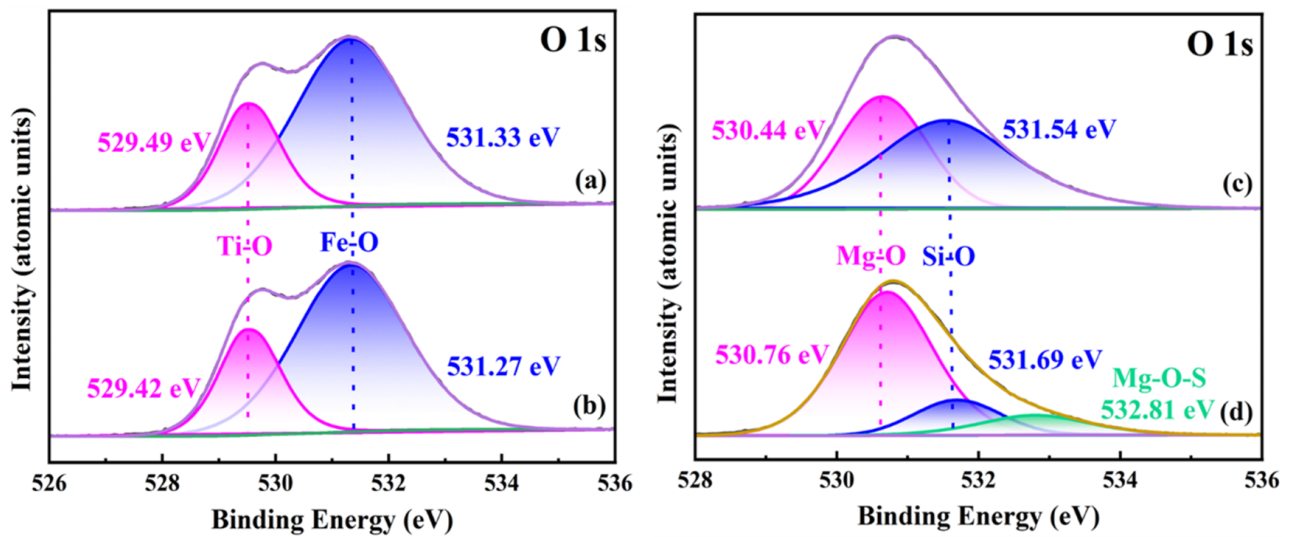


Figure 11. High-resolution O1s spectra of (a) ilmenite, (b) treated with DSS, (c) forsterite, and (d) treated with DSS.

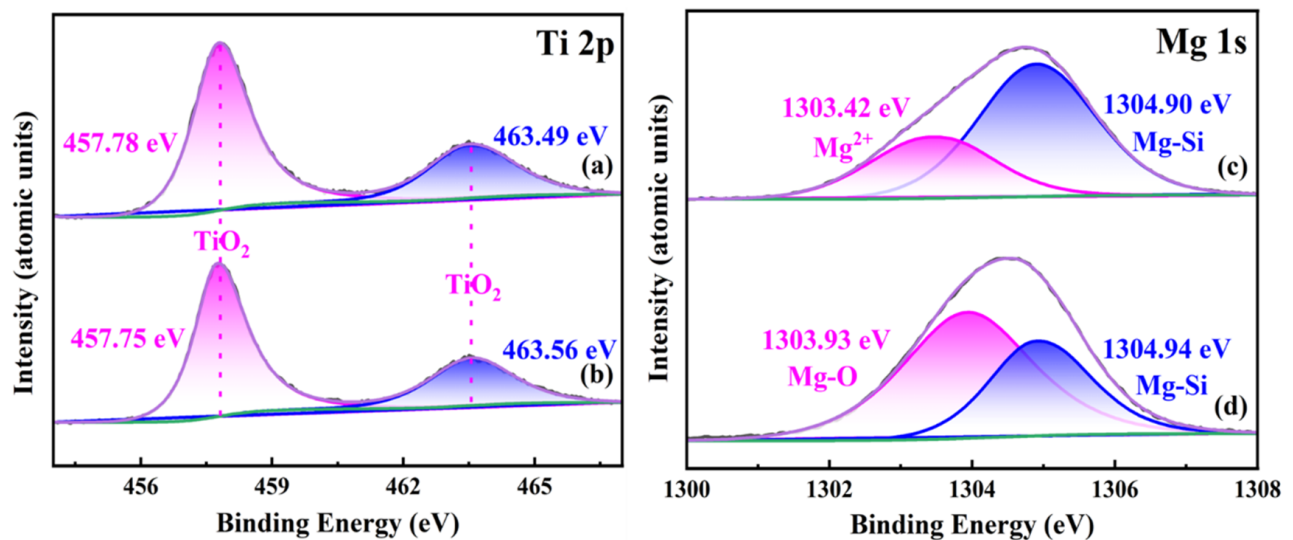
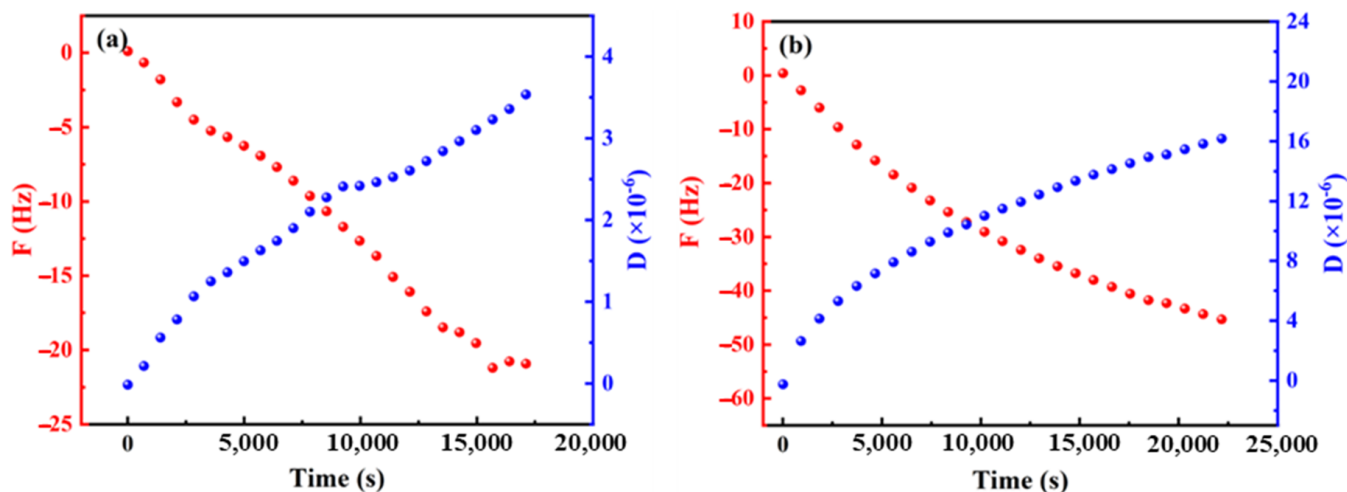


Figure 12. High-resolution Ti 2p spectra of (a) ilmenite, (b) treated with DSS, high-resolution Mg 1s spectra of (c) forsterite, and (d) treated with DSS.

### 3.3.5. Dynamic Adsorption Behavior of DSS on the Ilmenite/Forsterite Surface

As shown in Figure 13, the frequency ( $F$ ) sharply decreased to  $-59.74$  Hz, simultaneous with a sharp increase in dissipation ( $D$ ) on the forsterite sensor, whereas a slight decrease was observed on the ilmenite sensor. On the ilmenite sensor, a thin and rigid adsorption layer of DSS appeared to be forming, while the high  $D$  with  $16.48 \times 10^{-6}$  suggested the formation of a soft and dissipative adsorption layer on the forsterite sensor [45]. As seen in Table 3, at pH = 5.0, the mass density of the DSS adsorption layer was  $2578.38$  ng/cm<sup>2</sup> on the ilmenite surface and  $8204.62$  ng/cm<sup>2</sup> on the forsterite surface. The layer thickness was 25.78 nm and 82.05 nm, respectively. These findings indicated that DSS preferred to adsorb on the forsterite surface.



**Figure 13.** Adsorption frequency and energy dissipation of DSS on the surface of ilmenite and forsterite: (a) ilmenite, (b) forsterite.

**Table 3.** DSS adsorption data on ilmenite/forsterite sensor surface.

Sample	D ( $\times 10^{-6}$ )	F (Hz)	Thickness (nm)	Mass (ng/cm <sup>2</sup> )
Ilmenite	3.66	−21.51	25.78	2578.38
Forsterite	16.48	−45.68	82.05	8204.62

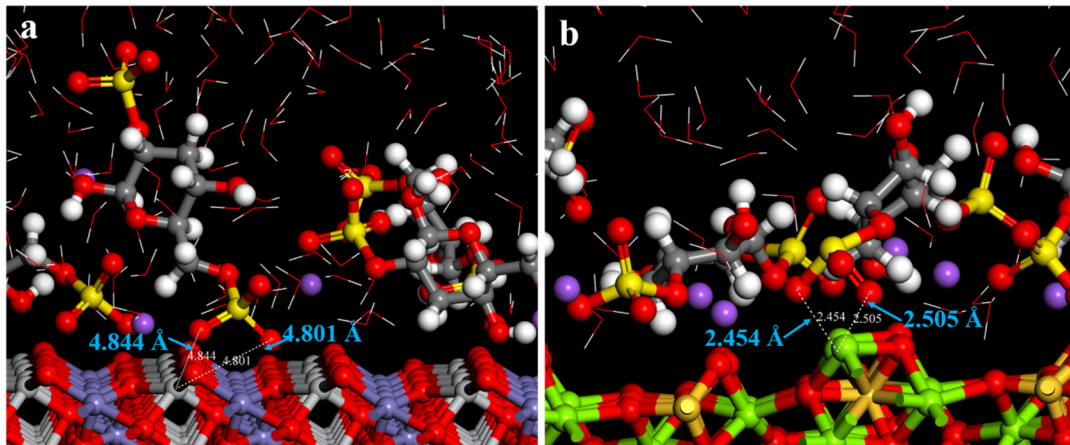
### 3.3.6. Adsorption Configuration of DSS on Ilmenite and Forsterite Surfaces

Figure 14 illustrates the DSS adsorption configuration on the surfaces of forsterite and ilmenite. The Mg site on the hydrated surface and the O atom in DSS produced two strong bonds, with lengths of 2.505 Å and 2.454 Å, respectively; the bond lengths with the Ti site were 4.844 Å and 4.801 Å, respectively. Since DSS is located at a distance from the mineral surface, there is little-to-no chemical contact between the active group and the mineral-surface active site [8]. Furthermore, Table 4 computes the interaction energy between DSS and the surfaces of forsterite and ilmenite. According to the table, DSS has a higher interaction energy, of −477.75 kJ/mol, with the surface of ilmenite than it does with the surface of forsterite (−989.06 kJ/mol). This suggests that DSS is more likely to adsorb on the surface of forsterite than it is on the surface of ilmenite [46,47]. This conclusion is in line with the findings of XPS, FT-IR, and AFM, demonstrating that DSS interacts with surfaces considerably more strongly on the surface of forsterite than it does on ilmenite.

**Table 4.** Interaction energy of DSS with mineral surfaces.

Sample	Interaction Energy (kJ/mol)
Ilmenite	−497.17
Forsterite	−805.85

The first peak in the distribution of O atoms and Mg atoms was located at 2.41 Å, whereas the nearest distance between O atoms and Si atoms was about 3.19 Å (Figure 15). These findings verified that DSS was chemisorbed with Mg active sites on the forsterite surface [48,49]. In agreement with the XPS data, the first peak of O-Ti and O-Fe were located at 3.25 Å and 3.39 Å, respectively, which implied that DSS interacted with the ilmenite surface by physisorption, via the Ti active site.



**Figure 14.** The adsorption configurations of DSS on ilmenite and forsterite surfaces: (a) ilmenite, (b) forsterite.

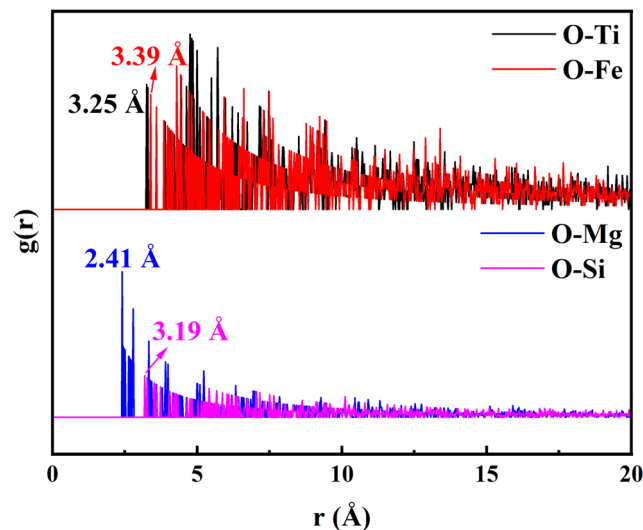


**Figure 15.** The radial distribution function of O-Metal.

#### 4. Conclusions

To effectively separate ilmenite and forsterite via flotation, the DSS was initially presented as a new depressant. Under the optimized conditions of pH = 5.0 and 10 mg/L DSS, the DSS showed a stronger selective depression on forsterite than ilmenite. The DSS depressant was chemisorbed strongly onto the forsterite surface via Mg active sites, whereas the weaker physisorption of DSS via Ti active sites was detected on the forsterite surface. The adsorption layer height and adsorption density of DSS with 8204.62 ng/cm<sup>2</sup> on the forsterite surface were larger than that of the ilmenite surface, which was 2578.38 ng/cm<sup>2</sup>. Based on the facts above, it can be said that DSS is now a more effective inhibitor than natural starch. This is due to the sulfuric acid group's strong polarity, which improves its solubility and dispersion in water, as well as the group's ability to selectively bond to metal atoms, which promotes the DSS's selective adsorption on gangue surfaces and allows for high inhibition and selectivity in the DSS. It offers recommendations for the selection of high-efficiency ilmenite separation inhibitors, and has a wide range of industrial application prospects for the effective separation of ilmenite and forsterite.

**Author Contributions:** G.F.: Writing—review and editing; H.Z.: methodology; F.T.: writing—original draft; H.W.: formal analysis; L.X.: methodology; Y.C.: methodology; H.X.: validation; F.Z.: validation;

J.H.: supervision; G.L.: writing—review and editing. All authors have read and agreed to the published version of the manuscript.

**Funding:** This research was funded by the National key research and development plan (Grant No. 2023YFC2908301), National Natural Science Foundation of China (No. U1908226; 52104270), China Postdoctoral Science Foundation project (No. 2022M710851), Key Specialized Research and Development Breakthrough Project in Henan Province (No. 221111320300), and Zhongyuan Critical Metals Laboratory (No. GJJSFGFYQ202329). This research received no external funding.

**Data Availability Statement:** Data are contained within the article.

**Conflicts of Interest:** The authors declare no conflict of interest.

## References

1. Desheng, C.; Longsheng, Z.; Tao, Q.; Guoping, H. Desilication from titanium–vanadium slag by alkaline leaching. *Trans. Nonferrous Met. Soc. China* **2013**, *23*, 3076–3082. [[CrossRef](#)]
2. Samal, S.; Mohapatra, B.K.; Mukherjee, P.S.; Chatterjee, S.K. Integrated XRD, EPMA and XRF study of ilmenite and titania slag used in pigment production. *J. Alloys Compd.* **2009**, *474*, 484–489. [[CrossRef](#)]
3. Zhao, W.; Chen, J.; Chang, X.; Guo, S. Effect of microwave irradiation on selective heating behavior and magnetic separation characteristics of Panzhihua ilmenite. *Appl. Surf. Sci.* **2014**, *300*, 171–177. [[CrossRef](#)]
4. Deng, R.; Yang, X.; Hu, Y.; Ku, J. Effect of Fe(II) as assistant depressant on flotation separation of scheelite from calcite. *Miner. Eng.* **2018**, *118*, 133–140. [[CrossRef](#)]
5. Fan, G.; Zhang, C.; Wang, T.; Deng, J.; Cao, Y.; Chang, L.; Zhou, G.; Wu, Y.; Li, P. New insight into surface adsorption thermodynamic, kinetic properties and adsorption mechanisms of sodium oleate on ilmenite and titanite. *Adv. Powder Technol.* **2020**, *31*, 3628–3639. [[CrossRef](#)]
6. Fan, X.; Rowson, N.A. The effect of Pb(NO<sub>3</sub>)<sub>2</sub> on the ilmenite flotation. *Miner. Eng.* **2000**, *13*, 205–215. [[CrossRef](#)]
7. Meng, Q.; Yuan, Z.; Yu, L.; Xu, Y.; Du, Y. Study on the activation mechanism of lead ions in the flotation of ilmenite using benzyl hydroxamic acid as collector. *J. Ind. Eng. Chem.* **2018**, *62*, 209–216. [[CrossRef](#)]
8. Kang, Y.; Zhang, C.; Wang, H.; Xu, L.; Li, P.; Li, J.; Li, G.; Peng, W.; Zhang, F.; Fan, G.; et al. A novel sodium trans-2-nonene hydroxamate for the flotation separation of ilmenite and forsterite: Superior collecting and selectivity. *Sep. Purif. Technol.* **2024**, *333*, 125830. [[CrossRef](#)]
9. Liu, X.; Huang, G.Y.; Li, C.X.; Cheng, R.J. Depressive effect of oxalic acid on titanite during ilmenite flotation. *Miner. Eng.* **2015**, *79*, 62–67. [[CrossRef](#)]
10. Zhao, X.; Meng, Q.Y.; Yuan, Z.T.; Zhang, Y.; Li, L. Effect of sodium silicate on the magnetic separation of ilmenite from titanite by magnetite selective coating. *Powder Technol.* **2019**, *344*, 233–241. [[CrossRef](#)]
11. Yang, Y.H.; Xu, L.H.; Tian, J.; Liu, Y.C.; Han, Y.X. Selective flotation of ilmenite from olivine using the acidified water glass as depressant. *Int. J. Miner. Process.* **2016**, *157*, 73–79. [[CrossRef](#)]
12. Qian, Y.; Wang, Z.; Cao, J. New depression mechanism of polymeric depressant on titanite in ilmenite flotation. *Sep. Purif. Technol.* **2021**, *264*, 118468. [[CrossRef](#)]
13. Yang, S.; Xu, Y.; Liu, C.; Huang, L.; Huang, Z.; Li, H. The anionic flotation of fluorite from barite using gelatinized starch as the depressant. *Colloids Surf. A Physicochem. Eng. Asp.* **2020**, *597*, 124794. [[CrossRef](#)]
14. Yang, S.; Wang, L. Measurement of froth zone and collection zone recoveries with various starch depressants in anionic flotation of hematite and quartz. *Miner. Eng.* **2019**, *138*, 31–42. [[CrossRef](#)]
15. Ludovici, F.; Hartmann, R.; Rudolph, M.; Liimatainen, H. Thiol-Silylated Cellulose Nanocrystals as Selective Biodepressants in Froth Flotation. *ACS Sustain. Chem. Eng.* **2023**, *11*, 16176–16184. [[CrossRef](#)] [[PubMed](#)]
16. Wang, W.; Wang, H.; Wu, Q.; Zheng, Y.; Cui, Y.; Yan, W.; Deng, J.; Peng, T. Comparative study on adsorption and depressant effects of carboxymethyl cellulose and sodium silicate in flotation. *J. Mol. Liq.* **2018**, *268*, 140–148. [[CrossRef](#)]
17. Yuan, Z.; Zhao, X.; Meng, Q.; Zhang, Y.; Xu, Y.; Li, L. Adsorption mode of sodium citrate for achieving effective flotation separation of ilmenite from titanite. *Miner. Eng.* **2021**, *171*, 107086. [[CrossRef](#)]
18. Meng, Q.; Yuan, Z.; Yu, L.; Xu, Y.; Du, Y.; Zhang, C. Selective depression of titanite in the ilmenite flotation with carboxymethyl starch. *Appl. Surf. Sci.* **2018**, *440*, 955–962. [[CrossRef](#)]
19. Wang, Z.; Xu, R.; Wang, L. Adsorption of polystyrenesulfonate on titanite surface: Experiments and quantum chemical calculations. *J. Mol. Liq.* **2020**, *319*, 114167. [[CrossRef](#)]
20. Yang, B.; Zhu, Z.; Sun, H.; Yin, W.; Hong, J.; Cao, S.; Tang, Y.; Zhao, C.; Yao, J. Improving flotation separation of apatite from dolomite using PAMS as a novel eco-friendly depressant. *Miner. Eng.* **2020**, *156*, 106492. [[CrossRef](#)]
21. Cao, Z.; Cao, Y.; Qu, Q.; Zhang, J.; Mu, Y. Separation of bastnaesite from fluorite using ethylenediamine tetraacetic acid as depressant. *Miner. Eng.* **2019**, *134*, 134–141. [[CrossRef](#)]
22. Xu, Y.; Yuan, Z.; Meng, Q.; Zhao, X.; Du, Y. Study on the flotation behavior and interaction mechanism of ilmenite with mixed BHA/NaOL collector. *Miner. Eng.* **2021**, *170*, 107034. [[CrossRef](#)]

23. Du, Y.; Meng, Q.; Yuan, Z.; Xu, Y.; Li, L. New cognitions into three new classified titanogite in mineralogical characteristics and fundamental performances. *Miner. Eng.* **2021**, *169*, 106962. [[CrossRef](#)]
24. Mehdilo, A.; Irannajad, M.; Rezai, B. Effect of crystal chemistry and surface properties on ilmenite flotation behavior. *Int. J. Miner. Process.* **2015**, *137*, 71–81. [[CrossRef](#)]
25. Meng, Q.; Yuan, Z.; Li, L.; Lu, J.; Yang, J. Modification mechanism of lead ions and its response to wolframite flotation using salicylhydroxamic acid. *Powder Technol.* **2020**, *366*, 477–487. [[CrossRef](#)]
26. Yuan, Z.; Zhao, X.; Meng, Q.; Zhang, Y. Investigation of selective adsorption of sodium oleate during separation of ilmenite from titanogite via surface magnetization. *Miner. Eng.* **2021**, *171*, 107128. [[CrossRef](#)]
27. Zhang, C.; Li, P.; Cao, Y.; Hao, H. Synthesis of sodium oleate hydroxamate and its application as a novel flotation collector on the ilmenite-forsterite separation. *Sep. Purif. Technol.* **2022**, *284*, 120283. [[CrossRef](#)]
28. Tazikeh, S.; Kondori, J.; Zendejboudi, S.; Amin, J.S. Molecular dynamics simulation to investigate the effect of polythiophene-coated Fe<sub>3</sub>O<sub>4</sub> nanoparticles on asphaltene precipitation. *Chem. Eng. Sci.* **2021**, *237*, 116417. [[CrossRef](#)]
29. Xu, L.; Hu, Y.; Dong, F.; Gao, Z. Anisotropic adsorption of oleate on diasporite and kaolinite crystals: Implications for their flotation separation. *Appl. Surf. Sci.* **2014**, *321*, 331–338. [[CrossRef](#)]
30. Hao, H.; Li, L.; Yuan, Z.; Liu, J. Molecular arrangement of starch, Ca<sup>2+</sup> and oleate ions in the siderite-hematite-quartz flotation system. *J. Mol. Liq.* **2018**, *254*, 349–356. [[CrossRef](#)]
31. Hao, Z.; Jiankun, W.; Wenjing, L.; Fengyan, L. Microwave-assisted synthesis, characterization, and textile sizing property of carboxymethyl corn starch. *Fibers Polym.* **2015**, *16*, 2308–2317. [[CrossRef](#)]
32. Saboktakin, M.R.; Tabatabaie, R.M.; Maharramov, A.; Ramazanov, M.A. Synthesis and characterization of new electrorheological fluids by carboxymethyl starch nanocomposites. *Carbohydr. Polym.* **2010**, *79*, 1113–1116. [[CrossRef](#)]
33. Yuan, Z.; Du, Y.; Meng, Q.; Zhang, C.; Xu, Y.; Zhao, X. Adsorption differences of carboxymethyl cellulose depressant on ilmenite and titanogite. *Miner. Eng.* **2021**, *166*, 106887. [[CrossRef](#)]
34. Chen, W.; Feng, Q.; Zhang, G.; Yang, Q. The flotation separation of scheelite from calcite and fluorite using dextran sulfate sodium as depressant. *Int. J. Ofmineral Process.* **2017**, *169*, 53–59. [[CrossRef](#)]
35. Liu, W.; Zhang, J.; Wang, W.; Deng, J.; Chen, B.; Yan, W.; Xiong, S.; Huang, Y.; Liu, J. Flotation behaviors of ilmenite, titanogite, and forsterite using sodium oleate as the collector. *Miner. Eng.* **2015**, *72*, 1–9. [[CrossRef](#)]
36. Rhein, F.; Zhai, O.; Schmid, E.; Nirschl, H. Multidimensional Separation by Magnetic Seeded Filtration: Experimental Studies. *Powders* **2023**, *2*, 588–606. [[CrossRef](#)]
37. Dong, L.; Jiao, F.; Qin, W.; Hailing, Z.; Wenhao, J. New insights into the carboxymethyl cellulose adsorption on scheelite and calcite: Adsorption mechanism, AFM imaging and adsorption model. *Appl. Surf. Sci.* **2019**, *463*, 105–114. [[CrossRef](#)]
38. Liu, Q.; Zhang, Y.; Laskowski, J.S. The adsorption of polysaccharides onto mineral surfaces: An acid/base interaction. *Int. J. Miner. Process.* **2000**, *60*, 229–245. [[CrossRef](#)]
39. Daou, T.J.; Begin, S.C.; Greneche, J.M.; Thomas, F.; Derory, A.; Bernhardt, P.; Legaré, P.; Pourroy, G. Phosphate adsorption properties of magnetite-base nanoparticles. *Chem. Mater.* **2007**, *19*, 4494–4505. [[CrossRef](#)]
40. Ouerd, A.; Dumont, C.A.; Berthome, G.; Normand, B. Reactivity of titanium in physiological medium: I. Electrochemical characterization of the metal/protein interface. *J. Electrochem. Soc.* **2007**, *154*, 593–601. [[CrossRef](#)]
41. Sugiyama, S.; Miyamoto, T.; Hayashi, H.; Moffat, J.B. Oxidative coupling of methane on mgo-mgso<sub>4</sub> catalysts in the presence and absence of carbon tetrachloride. *Bull. Chem. Soc. Jpn.* **1996**, *69*, 235–240. [[CrossRef](#)]
42. Haycock, D.E.; Kasrai, M.; Nicholls, C.J.; Urch, D.S. ChemInform abstract: The electronic structure of magnesium hydroxide (brucite) using X-ray emission, X-ray photoelectron, and auger spectroscopy. *Chem. Informationsdienst* **1979**, *10*, 1791–1796. [[CrossRef](#)]
43. Seyama, H.; Soma, M. Bonding-state characterization of the constituent elements of silicate minerals by X-ray photoelectron spectroscopy. *Chem. Informationsdienst* **1985**, *16*, 2199–2924.
44. Seyama, H.; Soma, M. X-ray Photoelectron Spectroscopic Study of Montmorillonite Containing Exchangeable Divalent Cations. *J. Am. Chem. Soc.* **1984**, *80*, 237–248. [[CrossRef](#)]
45. Wu, B.; Raghavan, S. Removal of BTA Adsorbed on Cu: A Feasibility Study Using the Quartz Crystal Microbalance with Dissipation (QCMD) Technique. *ECS J. Solid State Sci. Technol.* **2019**, *8*, P3114–P3117. [[CrossRef](#)]
46. Gao, F.; Dong, L.; Xue, Z.; Cai, S.; Fan, M.; Hao, B.; Fan, P.; Bao, W.; Wang, J. Dodecylamine enhanced coal gasification fine slag flotation and its molecular dynamics simulation. *Miner. Eng.* **2023**, *203*, 108322. [[CrossRef](#)]
47. Tang, Y.; Kelebek, S.; Yin, W. Surface chemistry of magnesite and calcite flotation and molecular dynamics simulation of their cetyl phosphate adsorption. *Colloids Surf. A Physicochem. Eng. Asp.* **2020**, *603*, 125246. [[CrossRef](#)]
48. Wang, L.; Li, Z.; Zhang, H.; Lyu, W.; Zhu, Y.; Ma, Y.; Li, F. The role of gellan gum in the selective flotation separation of fluorite from calcite: An experimental and molecular dynamics simulation study. *Powder Technol.* **2024**, *432*, 119156. [[CrossRef](#)]
49. Huang, H.; Gao, W.; Li, X. Effect of SO<sub>4</sub><sup>2-</sup> and PO<sub>4</sub><sup>3-</sup> on flotation and surface adsorption of dolomite: Experimental and molecular dynamics simulation studies. *Colloids Surf. A Physicochem. Eng. Asp.* **2024**, *680*, 132699. [[CrossRef](#)]

**Disclaimer/Publisher's Note:** The statements, opinions and data contained in all publications are solely those of the individual author(s) and contributor(s) and not of MDPI and/or the editor(s). MDPI and/or the editor(s) disclaim responsibility for any injury to people or property resulting from any ideas, methods, instructions or products referred to in the content.